What do we gain from multiple q-shell acquistions in high angular resolution diffusion imaging?

Jonas Cordes[1], Peter Neher[1], Hans-Peter Meinzer[1], Bram Stieltjes[2], and Klaus Maier-Hein[1,2]

[1]*Medical and Biological Informatics, German Cancer Research Center (DKFZ), Heidelberg, Baden-Württemberg, Germany,* [2]*Quantitative Image-based Disease Characterization, German Cancer Research Center (DKFZ), Heidelberg, Baden-Württemberg, Germany*

Purpose: At high b-value q-shells, HARDI datasets exhibit a high angular resolution at the cost of a low signal-to-noise ratio (SNR).[1] Low b-value q-shells yield a low angular resolution and a high SNR. The most common reconstruction techniques are only designed for a single q-shell and only few methods have been proposed that take advantage of the combined information contained in multiple q-shell.[2] The benefit of acquiring multiple q-shell data in comparison to single q-shell data and different gradient-schemes is still unclear. In this work we want analyze weather the investment of parts of the scan time in acquisition of additional q-shells is beneficiary in comparison to single q-shell data.

Methods: Using Fiberfox, we obtained synthetic diffusion weighted datasets simulated using a zeppelin and stick model for the intra- and inter-axonal compartment and a ball model for the extra-axonal compartment.[3,4] Several datasets with a two-strand fiber configuration and a crossing angle increasing in 5º steps from 0º to 90º were generated over an area of 15x15x3 voxels. The acquisition of each dataset was simulated multiple times with the same number of gradients distributed over distinct sets of q-shells. For single q-shell data we used 300 gradient directions with a constant b-value of S1=1000, S2=3000 and S3=6000 s/mm^2 respectively. For the multiple q-shell data we chose the same number and directions of gradients in a staggered configuration with the number of gradients per q-shell being linearly dependent on the b-value [M1=(1000,2000,3000); M2=(1000,2000,6000); M3=(1000,3000,5000)]s/mm^2.[6,11] Rician noise was added to yield an SNR of 30. The multiple q-shell signal is fitted for each gradient direction independently using $\ln(S(b)) = \ln(S(0)) - bD_{app} + (bD_{app})^2 K_{app}$, where S(b) is the measured signal, D_{app} is the apparent diffusion coefficient and K_{app} is the apparent diffusional kurtosis.[5] The maximum b-value of a multiple q-shell dataset is then used to generate new single q-shell datasets (M1*, M2*, M3*). The constant solid angle Q-Ball reconstruction with a spherical harmonic (SH) order of 12 and regularization λ of 0.006 is used for estimating the ODF.[1] By sampling the ODF for local maxima and a subsequent clustering, the principal diffusion directions are extracted. The distinction of the two diffusion directions was deemed reliable when the two peaks could be discerned in at least 95% of the voxels. This *minimum angle* marks the start of the curves in Figure 1a and 1b. *Peak accuracy* of a dataset is defined as the angular error between the mean peak and the ground-truth. *Peak precision* of a dataset is defined as the mean deviation of the individual peaks from the mean peak. As for the ODF peaks, we evaluated the ODF surface accuracy and precision for each dataset. As a similarity measure for ODF surfaces, we used the L^2 norm of the difference vector between the corresponding SH coefficient vectors c_1 and c_2: $d(c_1,c_2) = \sqrt{\sum_{k=1}^{K}(c_1^k - c_2^k)^2}$ where K is the number of SH coefficients.[6] The *surface accuracy* for one dataset is thus defined as $d(\bar{c}, c_{ref})$ where $\bar{c}$ is the corresponding mean SH coefficient vector and c_{ref} is the ground-truth SH coefficient vector, which were derived from the ODF reconstructed from a noiseless single shell dataset with a b-value of 6000 s/mm^2 (S3). The *surface precision* is defined as the average deviation of the SH coefficient vectors of one dataset to the corresponding mean coefficient vector $\bar{c}$: $\frac{1}{n}\sum_{n=1}^{N} d(c_n, \bar{c})$.

Results: The minimum angle between the diffusion main peaks that could be recovered by the above-described procedure is 30º for the multi q-shell datasets and for single q-shell with high b-value (starting point of curve M1*, M2*, M3*, S3 in Figure 1a, 1b). All three multiple q-shell datasets share a high peak accuracy beneath an error of <1.5º for resolving the 30º crossings. From 30º to 90º, the peak accuracy increases further with an error < 0.6º. A value of 1.75º ± 0.75º could be reached for peak precision (Figure 1b), which is worse than the peak precision of S3 but around the peak precision of S2. The ODF surfaces accuracy (Figure 2a) is improved by adding low b-value q-shells to high b-value datasets (Figure 2a - M3*, M2*). For the multiple q-shell datasets a slight decrease of surface precision (Figure 2b) is observable compared to the single q-shell datasets. Furthermore we found that a multiple q-shell acquisition with a maximum b-value of 3000 s/mm² (M1) yields a peak and surface accuracy that is comparable to that of a single shell acquisition at b=6000 s/mm² (S3).

Discussion: We showed that including low b-value q-shells into an acquisition with high b-values, results in a more accurate surface. Furthermore we showed that low b-values in a multi-shell configuration can be sufficient to reach the performance of high b-value single shell acquisitions. A detailed evaluation of the gradient scheme configurations[6], signal fitting[9], noise modeling[5] and alternative reconstruction methods[8] are of interest for further research. The presented methods may provide a good framework to perform such studies.

References: *1. D. Tuch, et al. 1999. Proceedings of the ISMRM, p. 321. 2. I. Aganj, et al. 2010. Magn Reson Med 64(2): 554-566. 3. E. Panagiotaki, et al. 2012. NeuroImage, 59:2241–2254. 4. P. F. Neher, et al. 2013. Magn Reson Med, Accepted for publication. 5. J. Jensen, et al. 2005. Magn Reson Med 53 (6), 1432–1440 6. A. Kamath, et al. 2012. MICCAI Workshop on Computational Diffusion MRI Nice. 7. I. Aganj, et al. 2009a. IEEE, pp. 1398–1401. 8 J. Tournier, et al. 2004. NeuroImage 23, 1179–1185. 9. T. Niendorf, et al. 1996. Magn Reson Med 36, 847–857 10. D.S. Tuch, 2004, Magn Reson Med, 52, pp. 1358–1372. 11. E.Caruyer, et al. 2013, Magn Reson Med.*

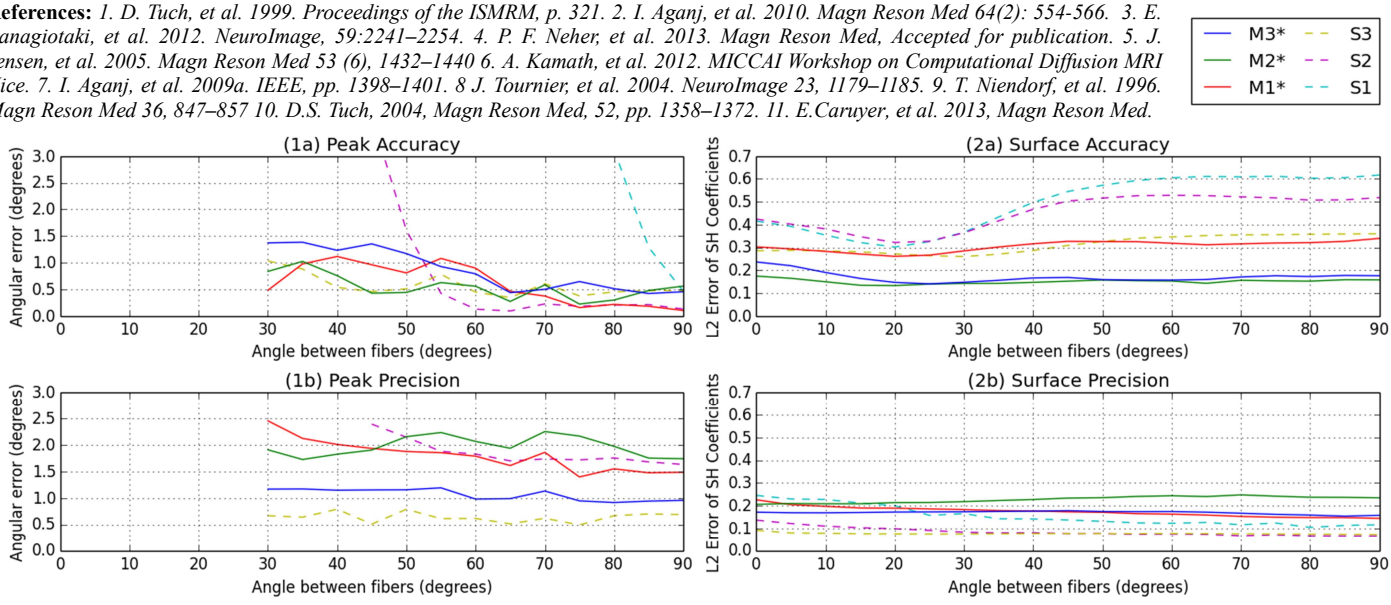

Figure 1: ODF peak accuracy (a) and peak precision (b) at different crossing angles. Figure 2: Surface Accuracy (a) and surface precision (b) at different crossing angles.